High-speed Atomic Force Microscopy Techniques for Observing Dynamic Biomolecular Processes

Daisuke Yamamoto[1,2], Takayuki Uchihashi[1,2], Noriyuki Kodera[1,2], Hayato Yamashita[1], Shingo Nishikori[3], Teru Ogura[2,3], Mikihiro Shibata[1], Toshio Ando*[1,2]

[1]Department of Physics, Kanazawa University, Kakuma-machi, Kanazawa 920-1192, Japan. [2]Core Research for Evolutional Science and Technology (CREST) of the Japan Science and Technology Agency, Sanban-cho, Chiyoda-ku, Tokyo 102-0075, Japan. [3]Department of Molecular Cell Biology, Institute of Molecular Embryology and Genetics, Kumamoto University, Kumamoto 860-0811, Japan.

*Corresponding author: tando@kenroku.kanazawa-u.ac.jp, Tel: +81 76-264-5663, Fax: +81 76-264-5739

Running Title: High-speed atomic force microscopy techniques

ABSTRACT

Atomic force microscopy enables direct visualization of single protein molecules in liquids at sub-molecular resolution. High-speed atomic force microscopy further makes it possible to visualize dynamic biomolecular processes at subsecond resolution. However, dynamic imaging of biomolecular processes imposes various requirements on "wet techniques" and imaging conditions, which are often different from those for static imaging. This article first surveys the imposed requirements, then focuses on practical techniques associated with dynamic imaging, highlighting the preparation of substrate surfaces, and presents examples of the use of these techniques.

1. Introduction

Single-molecule visualization of functional behavior of proteins has been performed using fluorescence microscopy (*e.g.*, Goldman, 2009; Joo *et al*., 2008; Park *et al*., 2007). This approach has enriched our knowledge of dynamic processes of proteins. However, even using fluorescence microscopy tools with a spatial resolution beyond the diffraction limit (Huang *et al*., 2009), it is impossible to observe protein molecules themselves since only single featureless fluorescent spots are observable. Therefore, we need to acquire additional information to bridge the gap between the behavior of fluorescent spots and the actual behavior of labeled protein molecules.

Atomic force microscopy (AFM) allows for the direct observation of individual protein molecules in solutions, at sub-molecular resolution. However, its imaging rate is too low to trace their dynamic behaviors. Rapidly moving molecules cannot be imaged at all. In the last decade, significant efforts have been carried out to increase the imaging rate of biological AFM (bio-AFM) (*e.g.*, Ando *et al*., 2001; Ando *et al*., 2008; Viani *et al*., 1999; Fantner *et al*., 2006). Only increasing the scan speed of AFM would not be difficult, if we ignore potential damage to the sample or disturbance of biomolecular processes. Very precise and fast control of the tip-sample distance is mandatory for observing delicate dynamic biomolecular processes. To achieve high-speed and low-invasive AFM imaging, various techniques have been devised (*e.g.*, Kodera *et al*., 2005, 2006) As a result, some dynamic events and structural changes in proteins have been successfully visualized (Ando *et al*., 2006; Yamamoto *et al*., 2008; Miyagi *et al*., 2008; Yamashita *et al*., 2009; Shibata *et al*., 2009). As comprehensive descriptions for realizing the instrumentation are already given elsewhere (Ando *et al*., 2008), we focus here on other critical aspects of dynamic AFM imaging.

Static AFM imaging of biological samples has been performed by many researchers, and various methods for this imaging have accumulated. On the other hand, dynamic AFM imaging of biological samples is rather new, and hence, methods and scan conditions specifically required for dynamic imaging are not yet found in the literature. Here, we introduce methods useful for dynamic AFM imaging, highlighting the preparation of substrate surfaces.

2. Survey of requirements for high-speed bio-AFM imaging

A substrate surface, on which a sample is placed, plays an important role in AFM imaging. It should be flat enough so that we can easily identify the molecules of interest deposited on it. To observe dynamically acting protein molecules under physiological conditions, the substrate surface must not firmly bind the molecules so that their physiological function is retained. However, the sample-surface interaction is essential to avoid too fast Brownian motion, particularly for single protein molecules isolated completely from other molecules. Dynamic AFM imaging requires much more defined conditions for the substrate surface than static AFM imaging does.

We also have to consider requirements for observing dynamic protein-protein interactions. Supposing that one species of protein dynamically interacts with a protein counterpart, only one but not the other can be immobilized to a substrate surface. If both are surface bound, they have almost no chance to interact with each other. Consequently, selective protein attachment to a surface is required. A dynamic protein-protein interaction implies that their association is weak. Tapping mode AFM is suitable for imaging fragile samples because little lateral force is exerted to the sample, while the tip taps the sample. This tapping should not disturb delicate protein-protein interactions. Ideally, we have to achieve a very weak tapping force without slowing the imaging speed.

Protein molecules exhibit Brownian motion alongside physiologically relevant dynamic conformational changes. In many cases, the purpose of observing the dynamic behavior of proteins is to detect physiologically relevant changes in protein conformation. We therefore have to be able to distinguish the two types of movement. Special means sometimes have to be implemented for this distinction, as well as a means to impede Brownian motion.

Biological membranes are very fluidic. When membrane proteins are not assembled into a large ensemble or anchored to an immobile entity, they diffuse rapidly in a membrane, so that there is no way to observe their structure even using high-speed AFM with the capacity to image at 33 frames/s for a scan range of 240 × 240 nm^2 (Yamashita *et al*., 2007). In this case, we need some means to slow down diffusion.

In the following sections, several solutions for the difficulties mentioned above are presented and their effects are exemplified.

3. Substrate surfaces

For AFM imaging, bare surfaces of mica and highly oriented polygraphite (HOPG), as well as gold-coated surfaces of these substrates or silicon have often been used. In aqueous solution, proteins do not attach to HOPG except for rare cases. Gold-coated surfaces are typically used for preparing self-assembled monolayers of molecules containing a thiol. Proteins can be immobilized to these monolayers when the constituting monolayer molecules also possess a reactive or functional group. Since the preparation methods and characterization of these monolayers are well

described elsewhere (Hinterdorfer and Dufrêne, 2006; Liu *et al*., 2008), we here only cover bare mica surfaces, mica surface-supported planar lipid bilayers, and streptavidin 2D crystals formed on lipid bilayers.

3.1. Bare mica surface

Mica (natural muscovite or synthetic fluorophlogopite) has frequently been used as a substrate owing to its surface flatness at the atomic level over a large area. It has a net negative charge and is therefore quite hydrophilic. A bare mica surface adsorbs various proteins by electrostatic interactions. Except in rare cases (*e.g*., GroEL attachment in an end-up orientation), the orientation of adsorbed proteins is not unique, and the selective attachment of a specific species of protein is not expected. A mica surface is useful for observing the dynamic processes of a single species of isolated protein or membrane proteins in native membrane fragments. We can control the affinity for a specific protein by varying the ionic strength, pH, or by adding divalent cations such as Mg^{2+}. Divalent cations can link negatively charged proteins to a negatively charged mica surface.

Mica disks are prepared from a mica sheet with thickness of < 0.1 mm by cutting holes using a sharp puncher. Serrated edge formation, which often accompanies partial cleavage of interlayer contacts in the disk, should be avoided. Hydrodynamic pressure produced by rapid scanning of the sample stage induces vibrations of the disk through movement of the cleaved sites. For high-speed imaging, the disk should be small (1-2 mm in diameter) to avoid generation of too large a hydrodynamic pressure (Ando *et al*., 2002). The following handling protocol is recommended:

1. Glue a mica disk to a sample stage using epoxy and wait until it has dried (~1-2 h).
2. Press a Scotch tape to the surface of the mica disk and then smoothly remove the tape from the mica. The top layer of the mica will be removed with the tape, which can be checked by inspecting the surface of the removed tape.
3. Place a sample solution on the freshly cleaved mica disk surface for 1-3 min, and then rinse with an appropriate buffer solution.
4. Judge the affinity of the sample for the mica surface by AFM imaging.
5. Find an appropriate solution condition by repeated imaging using different solutions (an example is shown in Fig.1 for myosin V). When the affinity is too weak, reduce the ionic strength or pH, or change the concentration of divalent cations.

3.2. Mica surface-supported planar lipid bilayers

Mica surface-supported planar lipid bilayers are useful for attaching proteins to their surfaces with a controlled affinity or selectivity. A membrane surface with zwitterionic polar head groups such as phosphatidyl choline (PC) and phosphatidyl ethanolamine (PE) is known to resist protein adsorption (Zhang *et al*., 1998; Vadgama, 2005). Various lipids with functional groups [*e.g*., biotin and Ni-NTA] on their polar heads are commercially available. They enable specific attachment of

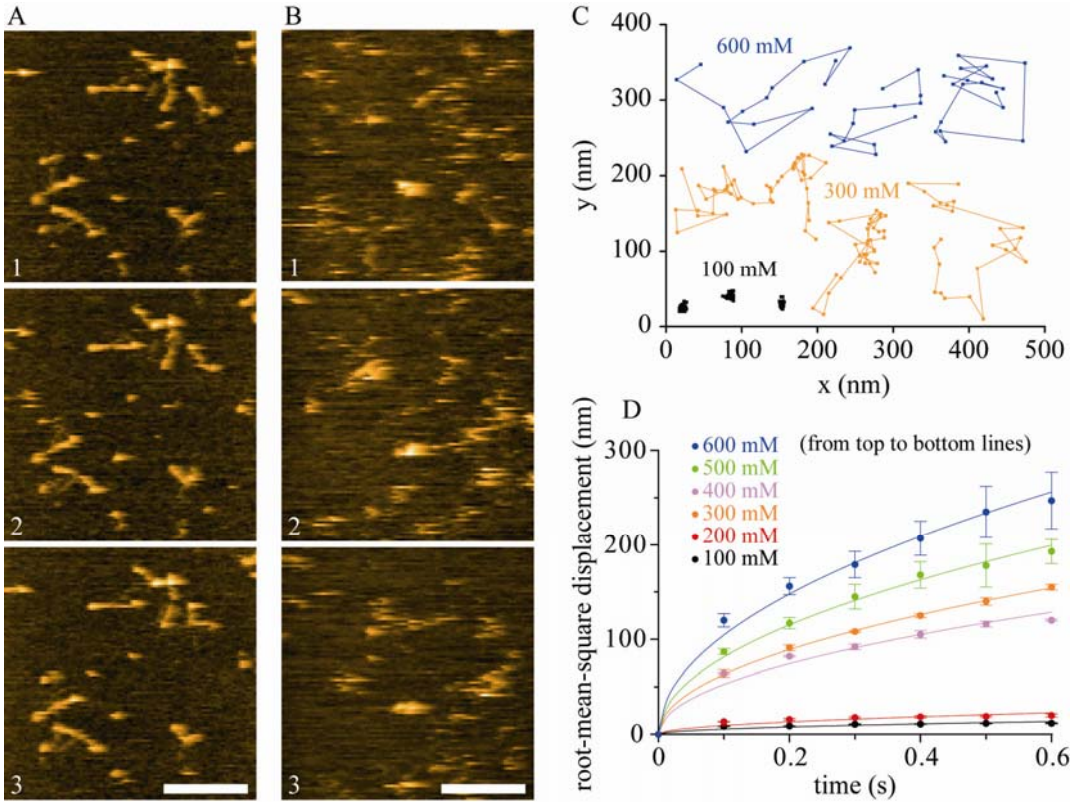

Figure 1. Ionic strength dependent diffusion of MyoV-HMM (tail-truncated myosin V) on bare mica surface. (A, B) Typical successive AFM images taken at 100 mM (A) and 600 mM KCl (B). Imaging rate: 102 ms/frame, scan area: 300×300 nm^2 with 100×100 pixels, scale bar: 100 nm. The number in each frame represents the frame number. The observation buffer is 20 mM imidazole-HCl (pH 7.6), 2 mM $MgCl_2$, 1 mM EGTA and 100 or 600 mM KCl. (C) Typical trajectories of MyoV-HMM measured in 100 mM, 300 mM or 600 mM KCl containing solutions. (D) Root-mean-square displacement (x_{rms}) as a function of time. Each point was calculated from the trajectories of ~100 molecules and well fitted by an equation $x_{rms} = \sqrt{4Dt}$, where D is the diffusion coefficient and t is the time elapse. The values of D [nm^2/s] at respective KCl concentrations are D_{100mM} = 79±10, D_{200mM} = 213±26, D_{300mM} = (0.99±0.01)×10^4, D_{400mM} = (0.69±0.04)×10^4, D_{500mM} = (1.69±0.04)×10^4 and D_{600mM} = (2.73±0.09)×10^4.

biotin- or His-tag-conjugated proteins to planar lipid bilayers. For electrostatic attachment, negatively charged head groups including phosphatidylserine (PS), phosphoric acid (PA), or phosphatidylglycerol (PG) and positively charged head groups such as trimethylammoniumpropane (TAP) and ethylphosphatidylcholine (EPC) are available. Unlike mica surfaces, the surface charge density can easily be controlled by mixing charged and neutral lipids in different ratios as long as no phase separation occurs.

3.2.1. Choice of alkyl chains

Dioleoyl-phosphatidyl-choline (DOPC) is useful for the preparation of 2D crystals of streptavidin and His-tag-labeled proteins when it is used in conjunction with biotinylated lipids and Ni-NTA-

containing lipids, respectively (Scheuring *et al*., 1999; Reviakine and Brisson, 2001). DOPC contains an unsaturated hydrocarbon in each of the two alkyl chains, which causes the bending of the chains and therefore weakens the interaction between neighboring DOPCs. This weak interaction lowers the phase-transition temperature of DOPC to ~ −20°C, thereby affording considerable fluidity to the planar bilayer at room temperature and facilitating the formation of 2D protein crystals. Such densely packed proteins do not diffuse easily. Dipalmitoyl-phosphatidyl-choline (DPPC) contains no unsaturated hydrocarbons in the alkyl chains. Therefore, its phase transition temperature is high (~41°C) and it is suitable for preparing planar lipid bilayers with low fluidity. For example, when planar bilayers are formed using DPPC at high temperature (~60°C) together with a suitable fraction of DPPE-biotin, streptavidin sparsely attached to the surface hardly diffuses at room temperature. When DOPE-biotin is used together with DPPC, the sparsely attached streptavidin diffuses at a moderate rate (Fig. 2).

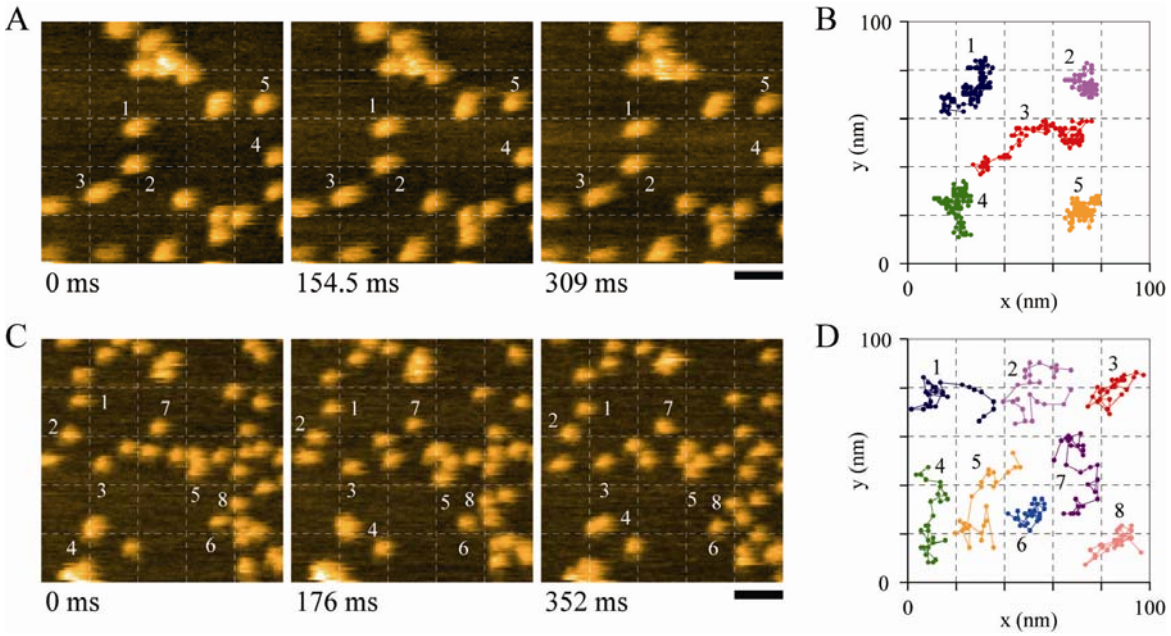

Figure 2. Mobility of lipid molecules monitored by diffusion of attached streptavidin molecules and its dependence on lipid compositions. Successive AFM images of streptavidin on lipid bilayers of DPPC + DPPE-biotin (9:1 w/w) and DPPC + DOPE-biotin (9:1 w/w) are shown in (A) and (C), respectively. Imaging rate: 154.5 ms/frame (A), 176 ms/frame (C), scan area, 200×200 nm^2 with 100×100 pixels, scale bar: 20 nm. The apparent difference in the size of streptavidin molecules between (A) and (C) is due to different cantilever tips. Trajectories of streptavidin molecules observed in (A) for ~15.6 s and (C) for ~4.6 s are plotted in (B) and (D), respectively. The numbers beside trajectories in (B) and (D) correspond to the numbered streptavidin molecules in (A) and (C), respectively.

3.2.2. Preparation of planar lipid bilayers

For the preparation of planar lipid bilayers on a mica surface, two methods are commonly used; the Langmuir-Blodgett method and the vesicle fusion method. In both cases, uniform and smooth

surfaces of lipid bilayers can be obtained. Here, we focus on the latter method, because of its simplicity and lack of a requirement for any expensive instruments and skills. Supported planar lipid bilayers are formed from small unilamellar vesicles by direct deposition of the solution on a freshly cleaved mica surface. Planar lipid bilayer formation proceeds through: (i) adsorption of small unilamellar vesicles on the mica surface, (ii) rupture of the vesicles and (iii) fusion of the resulting small membrane patches with juxtaposed lipid membranes. Although protocols for preparing lipid vesicles and supported lipid bilayers can be found elsewhere, we describe here a procedure routinely used in our laboratory.

1. Dissolve each lipid compound in chloroform or in a mixture of chloroform, methanol and water (follow the instructions provided by the manufacturers).
2. Mix lipid solutions at a desired ratio in a glass test tube.
3. Dry the organic solvent under a stream of N_2 gas. During this procedure, warm up the test tube by gripping it with your hand to facilitate solvent evaporation.
4. To ensure full evaporation, leave the test tube in a desiccator under aspirator vacuum for more than 30 min.
5. Add a buffer solution to the test tube (typical final concentration of lipids, 0.125 mM) and vortex it. If necessary, sonicate the test tube using an ultrasonic bath to disperse the lipids in the medium. At this stage, multilamellar lipid vesicles are formed. The lipid suspension is divided into small aliquots (~100 μL) and stored at –80 °C.
6. To obtain small unilamellar vesicles, sonicate the multilamellar vesicle suspension (typically 100 μL) with a tip sonicator at intervals of one second with a duty ratio of ~0.5 until the suspension becomes transparent (typically no more than 30 cycles).
7. Place a drop of the small unilamellar vesicle solution on a freshly cleaved mica surface and incuvate it for 30 min in a sealed container, while maintaining high humidity in the container to avoid sample drying by stuffing therein a piece of paper damped with water. Subsequently, rinse the sample with an appropriate buffer solution.
8. When the gel-liquid crystal transition temperature of the sample is higher than room temperature, warm up the sample in the sealed container slightly above the transition temperature for ~15 min.
9. Examples for lipid compositions [buffer conditions] are given below. The mixing ratios of lipids should be changed depending on the samples and dynamic events to be visualized.
   - highly fluidic bilayers with biotin; DOPC:DOPS:biotin-cap-DOPE = 7:2:1 (w/w) [10 mM HEPES-NaOH (pH 7.4), 150 mM NaCl and 2 mM $CaCl_2$].
   - low fluidic bilayers with biotin; DPPC:biotin-cap-DPPE = 9:1 (w/w) [10 mM HEPES-NaOH (pH 7.4), 150 mM NaCl and 2 mM $CaCl_2$].
   - slightly fluid bilayers with biotin; DPPC:biotin-cap-DOPE = 9:1 (w/w) [10 mM HEPES-NaOH (pH 7.4), 150 mM NaCl and 2 mM $CaCl_2$].

- highly fluidic bilayers with Ni-NTA; DOPC:DOPS:DOGS-NTA(Ni) =7:2:1 (w/w) [10 mM HEPES-NaOH (pH 7.4), 150 mM NaCl and 2 mM $CaCl_2$]
- low fluidic bilayers with Ni-NTA; DPPC:DOGS-NTA(Ni) = 9:1 (w/w) [50 mM Tris-HCl (pH 8.0), 50 mM KCl and 3 mM $MgCl_2$]
- low fluidic bilayers with positively charged head groups; DPPC:DPTAP = 7:3 (w/w) or only DPTAP [distilled water].
- low fluidic bilayers with negatively charged head groups; DPPG 100% [10 mM HEPES-NaOH (pH 7.4), 150 mM NaCl and 2 mM $CaCl_2$].
- low fluidic bilayers with negatively charged head groups formed on positively charged lipid bilayers; DPPA 100% [distilled water].

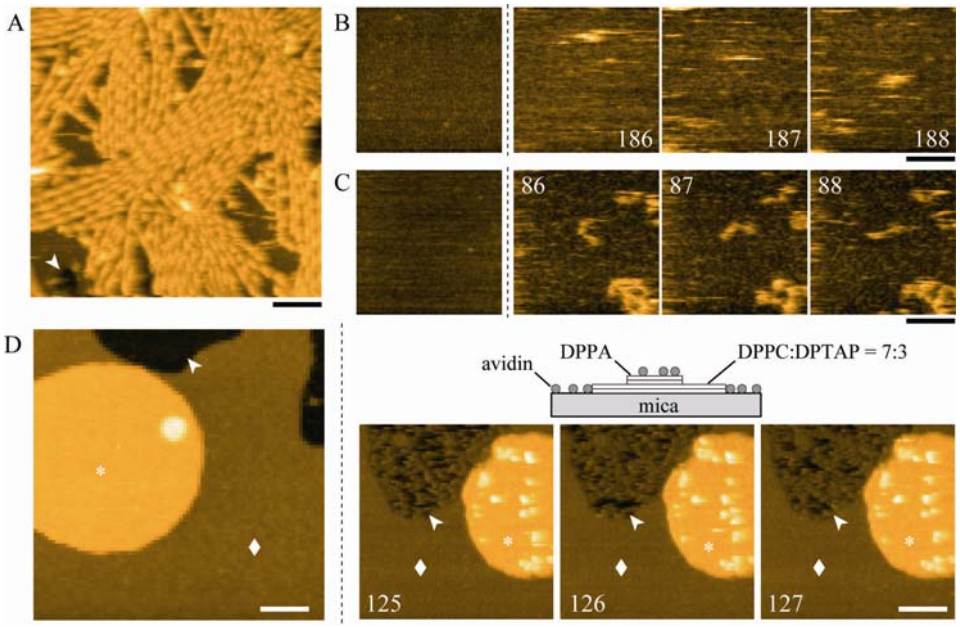

Figure 3. Electrostatic adsorption of proteins on charged lipid bilayers. (A) AFM image of actin filament paracrystal formed on positively charged lipid bilayers (DPPC:DPTAP = 7:3 w/w). The white arrowhead indicates an exposed mica surface. Scale bar, 100 nm. (B), (C) High-speed AFM images showing the effect of positive-charge surface density on the mobility of attached MyoV-HMM. The lipid compositions are (B) DPPC:DPTAP = 7:3 (w/w) and (C) only DPTAP. The leftmost AFM images show the surface of lipid bilayers before adding MyoV-HMM. Imaging rate, 101 ms/frame; scale bar, 100 nm. The number in each frame represents the frame number. MyoV-HMM was hardly visible (B) due to the large mobility, whereas it was visible (C) due to the low mobility. (D) AFM images of negatively charged lipid bilayers formed on positively charged lipid bilayers. The leftmost AFM image was taken before adding avidin (a positively charged protein). The white arrowhead, diamond and asterisk represent the surfaces of mica, positively charged lipid bilayers and negatively charged lipid bilayers, respectively (imaging rate: 418 ms/frame, scale bar: 100 nm). The remaining successive AFM images were taken after adding avidin (imaging rate: 175 ms/frame, scale bar: 100 nm). Avidin molecules are only observed on the negatively charged surfaces of mica and DPPA (see the upper schematic). The observation buffer contains 20 mM imidazole-HCl (pH 7.6), 25 mM KCl, 2 mM $MgCl_2$ and 1 mM EGTA.

3.2.3. Planar lipid bilayers as substrates

Electrostatic immobilization: Since the mica surface is negatively charged, positively charged lipid bilayers can easily be formed on the surface. Depending on the sample to be imaged, an appropriate positive-charge density has to be found by repeated imaging with various positive to neutral lipid ratios (examples are shown in Figs. 3A, B, and C). Negatively charged lipid bilayers can be formed in a wide area on a mica surface using DPPG (transition temperature [T_m], 41°C). Since the negative charge of DPPG is not positioned at the distal end of the polar head, the bilayer surface weakly adsorbs positively charged proteins. Thus far, negatively charged lipid bilayers have not been formed on a mica surface using DPPA (T_m = 67°C; the negative charge is positioned at the distal end of the polar head) or DPPS (T_m = 54°C). Another means is to form negatively charged lipid bilayers on positively charged bilayers. Although not completely successful yet, at least small patches of DPPA bilayers can be formed by this means (Fig. 3D).

Immobilization via specific interaction: Specific association pairs with strong affinities, such as [biotin and streptavidin] and [his-tag and Ni-NTA], can be used for selective immobilization of proteins. When relatively large molecules mediate the immobilization of a protein on lipid bilayers, the attached mediator would make it difficult to identify the immobilized protein. When streptavidin is used as a mediator, the use of streptavidin 2D crystals is recommended (see the next Section). Here, we show only an example of His-tag-conjugated protein immobilization. p97 is a hexameric ATPase of the AAA family and involved in cellular processes (more descriptions of p97 are given later). As shown in Fig. 4, recombinant p97 of which each subunit was conjugated with a His-tag was immobilized on a Ni-NTA-containing lipid bilayer. p97 was attached to the bilayer surface in a specific orientation due to the specific-site conjugation of a His-tag to each subunit.

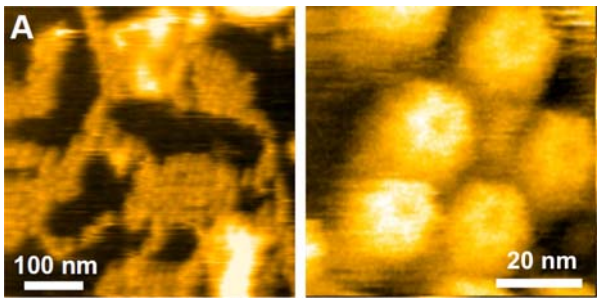

Figure 4. p97 attached on Ni-NTA-containing lipid bilayer through His-tag conjugated at the N-terminus of each subunit. (A) Segregation of Ni-NTA lipid in bilayer (p97 are densely packed at bright regions but absent in dark regions). (B) Ring structure of p97 (C-terminus D2 domain surface). Z-scales: (A) 20 nm, (B) 14 nm.

3.3. Streptavidin 2D crystals as substrates

2D crystals of streptavidin formed on biotin-containing lipid bilayers meet various requirements for substrate surfaces used in dynamic AFM imaging. Streptavidin is comprised of four identical

subunits, each of which specifically binds to one biotin molecule with a strong affinity ($Ka \approx 10^{13}$ M^{-1}) (Green, 1990). In 2D crystals, two biotin binding sites face the solution, and therefore, can bind to biotinylated samples to be imaged (Darst *et al*., 1991, Reviakine and Brisson, 2001). Since biotinylated Ni-NTA is commercially available, the surface can also bind to His-tag conjugated recombinant proteins. The surface roughness of a specific type of 2D crystal is very small, as mentioned later. Importantly, streptavidin is resistant to nonspecific binding of many proteins (Green, 1990), which safeguards the surface-bound proteins against dysfunction (Heyes *et al*., 2004) and allows the selective surface attachment of one species of protein in a multicomponent system. In addition, it allows protein attachment in a controlled orientation through the biotin or His-tag conjugation sites in the protein.

3.3.1. Preparation of streptavidin 2D crystals

On highly fluidic planar lipid layers containing a biotinylated lipid, streptavidin self-assembles into three distinct crystalline arrangements of *C*222, *P*2 and *P*1 symmetries, depending on the crystallization conditions such as pH (Wang *et al*., 1999) and ionic strength (Ratanabanangkoon and Gast, 2003), as described in the following. Note that all the 2D crystals have *P2* symmetry (Yamamoto *et al*., 2009) but we followed previous reports in the notation for the symmetry groups.

1. Crystallization buffer solutions: (*C*222 crystal) 10 mM HEPES-NaOH (pH 7.4), 150 mM NaCl and 2 mM $CaCl_2$; (*P*2 crystal) 10 mM MES-NaOH (pH 5.8), 450 mM NaCl and 2 mM $CaCl_2$; (*P*1 crystal) 10 mM acetate-NaOH (pH 4.0), 450 mM NaCl and 2 mM $CaCl_2$.
2. Prepare the mica-supported lipid planar bilayers containing biotin as mentioned in *Section* 3.2.2.
3. After washing the lipid planar bilayers with a crystallization buffer solution, place 0.1–0.2 mg/ml streptavidin in the crystallization buffer solution on the lipid bilayer and incubate at room temperature in a sealed container (keeping 100% relative humidity is a key to the successful crystallization with fewer defects).
4. After incubating at least for 2 h, wash out excess streptavidin with the crystallization buffer solution used.
5. If necessary, chemically fix the streptavidin crystals by applying a 10 mM glutaraldehyde-containing crystallization solution and incubate for 5 min. Then, quench the reaction using 20 mM Tris-HCl mixed in the crystallization buffer.

Fig. 5 (*top*) shows high-magnification AFM images of the three types of streptavidin crystals. Among the three, the *P*1 crystal shows the smallest surface roughness (Fig. 6C, *bottom*; RMS roughness ~0.14 nm) and the highest stability (Yamamoto *et al*., 2009). Even when tapped with an oscillating cantilever with relatively strong force, the crystal structure is unchanged, and hence, no chemical fixation is necessary. However, the *P*1 crystal often shows line cracks. The *C*222 crystal shows high uniformity over a wide area but similarly to the *P*2 crystal, its stability is lower than that of the *P*1 crystal, and therefore, chemical fixation is sometimes necessary. Its chemical fixation

does not significantly affect the affinity of streptavidin for biotin.

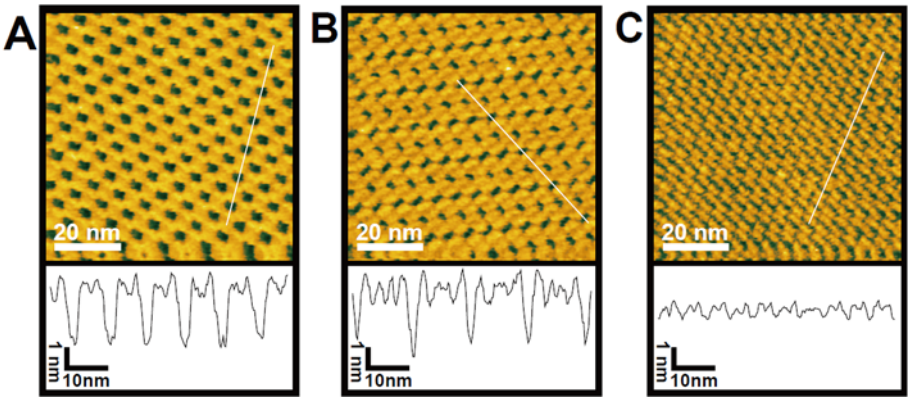

Figure 5. High magnification AFM images of the three types of streptavidin crystals (Yamamoto *et al*., 2009). The space group symmetries of the crystals are (A) *C*222, (B) *P*2 and (C) *P*1. (*top*) AFM images, according to previous reports (*P2* is a correct notation for all the crystals). (*bottom*) Surface profile along the lines indicated in the AFM images in *top*. The AFM images were obtained at an imaging rate of 1 s/frame with 256×256 pixels.

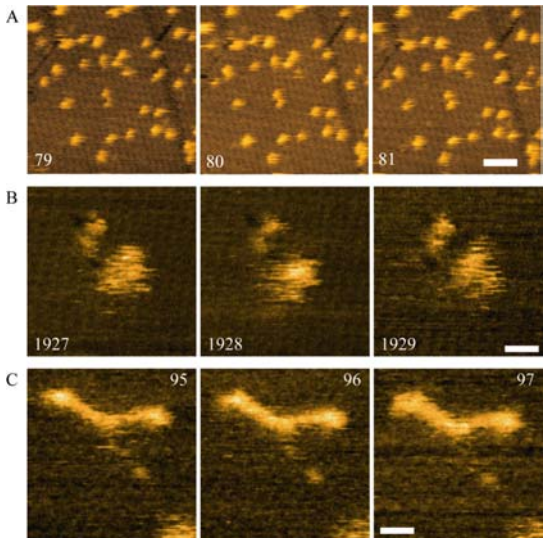

Figure 6. Biotinylated proteins attached onto streptavidin 2D crystal surfaces. (A) Successive AFM images of biotinylated calmodulin (CaM) attached on *P*1 crystal of streptavidin. The images do not reveal a typical dumbbell-like appearance of CaM because one of the two globes connected with a flexible central linker is not biotinylated. Scale bar, 20 nm. Imaging rate: 991 ms/frame, scan area: 100×100 nm^2 with 256×256 pixel, z-scale: 4.5 nm. The observation buffer is 20 mM imidazole-HCl (pH 7.6), 100 mM KCl, 2 mM $MgCl_2$, 1 mM EGTA. (B, C) Effect of the number of conjugated biotin per molecule on AFM image of MyoV-HMM immobilized on streptavidin 2D crystal. MyoV-HMM containing biotinylated CaM was immobilized on the *C222* crystal of streptavidin. Scale bar: 20 nm, imaging rate: 487 ms/frame, scan area: 100×100 nm^2 with 128×128 pixels, z-scale: 8.0 nm. The observation buffer was 20 mM Tris-HCl (pH 6.8), 100 mM KCl, 2 mM $MgCl_2$, 1 mM EGTA and 5 mM DTT. (B) MyoV-HMM having biotinylated CaM only at one of the two necks. It does not show the typical molecular shape because the unbiotinylated head moves rapidly and even the biotinylated head rotates rapidly around the biotin-linker. (C) MyoV-HMM with biotinylated CaM at both necks.

3.3.2. Use of streptavidin 2D crystals as substrates

Supposing that a protein to be imaged is relatively rigid and does not possess flexible chains, its biotinylated species immobilized on a streptavidin 2D crystal surface would not exhibit rapid Brownian motion even when only one biotin per molecule is introduced. If it rapidly rotates around the biotinylated site due to a flexible linker contained in the biotin compound used, we can use reactive dibiotin compounds for less mobility. However, when a protein to be imaged contains a flexible moiety and is biotinylated only at one site, it certainly exhibits too rapid Brownian motion to be imaged (examples are shown in Fig.6 for calmodulin (CaM) and tail-truncated myosin V [MyoV-HMM]). This rapid motion can be stopped by introducing biotin to the protein at more than two sites (Fig. 6C). Thus, the streptavidin 2D crystals are excellent substrates for oligomerized proteins as exemplified below but their usefulness is limited for monomeric proteins with flexible polypeptide chains.

We can specifically place a protein on streptavidin 2D crystals in a desired orientation when the protein is biotinylated at designed sites. For example, the D490C GroEL mutant, in which biotin is conjugated to the Cys-490 located at the outer surface of the equatorial domain, can attach to the *C*222 crystal surface in a side-on orientation (Fig. 7) (Yamamoto *et al*., 2009). In this orientation, both rings of GroEL are accessible to GroES floating in bulk solution. GroES never attaches to the crystal surface even when the concentration is increased to the 10 μM range, allowing for the observation of dynamic events of association/dissociation of the GroEL/GroES complex. Fig. 7 (*asterisks*) shows such a dynamic event in the presence of ADP.

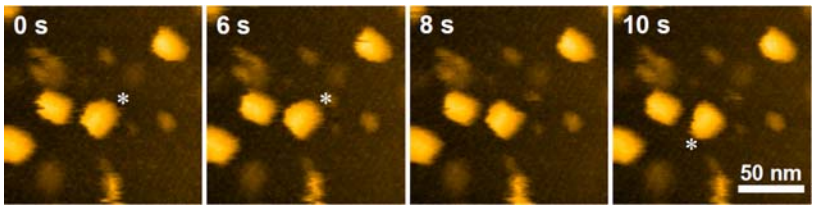

Figure 7. AFM images of the GroEL-GroES complex (Yamamoto *et al*., 2009). The D490C GroEL mutant was biotinylated at the outer surface of the equatorial domain, and was immobilized in a side-on orientation on a streptavidin *C*222 crystal that is chemically fixed with glutaraldehyde. The GroEL-GroES complex was formed and imaged in the buffer containing 1 μM GroES and 1 mM ADP. The asterisks indicate GroES bound to one of the GroEL rings. The AFM images were obtained at an imaging rate of 2 s/frame with 200×200 pixels. Z-scale: 19 nm.

4. Control of diffusional mobility

Proteins that are weakly and sparsely attached to a substrate surface often exhibit rapid Brownian motion. Even when densely packed on highly fluidic planar lipid bilayers, some proteins hardly form 2D crystals due to weak association or repulsion between protein molecules. Non-crystalline proteins diffuse due to the fluidity of the lipid bilayers, making it difficult to capture an

image. Depending on the situation, we need a specific means to impede the rapid diffusion, as detailed in the following.

1. Brownian motion of a protein that is attached to a surface by electrostatic interaction can be impeded by strengthening the interaction using a low ionic strength solution (Fig. 1) or a more charged surface (Fig. 3A). This approach is easy and effective for a large number of samples as the stronger electrostatic association usually does not hamper protein function. However, when it does, there are no ideal means to slow down the Brownian motion. One compromise is to place, with an appropriate surface density, small particles on the surface that have a relatively strong affinity for the surface. Diffusion of the protein molecules is slowed down by the contact with the particles. Using this means, we succeeded to visualize the step process of myosin V (MyoV) along actin tracks (unpublished).
2. When a protein hardly forms 2D crystals on a highly fluidic lipid bilayer, change the pH to reduce the electrostatic repulsion (an example is shown below), or place the non-crystalline protein on low fluidic lipid bilayers as exemplified in Fig. 2..
3. For membrane proteins embedded in native lipid membranes, their rapid diffusion sometimes can be impeded using Annexin (Ichikawa, 2006). Annexins are a protein family that bind to negatively charged phospholipids in the presence of calcium and assemble as trimers (Richter, 2005). Annexin A-V forms 2D crystals on PS-containing lipid membranes (Fig. 8A). Using this property, Annexin A-V can be used to trap membranes proteins in the defect sites of an Annexin 2D crystal. Although not native membrane proteins, streptavidin molecules are demonstrated to be trapped in the defects of the Annexin A-V crystal formed on very fluidic lipid bilayers (Fig. 8B). Without Annexin A-V, no image of streptavidin molecules can be taken due to rapid diffusion (Fig. 8C).

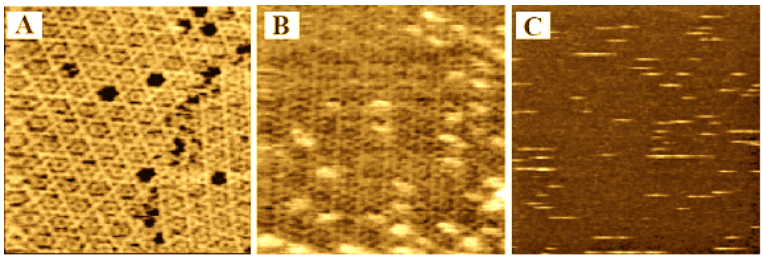

Figure 8. (A) An AFM image of the annexin A-V two-dimensional crystal on lipid bilayer. The lipid bilayer is composed of 65% DOPC, 34% DOPS and 1% biotin-capped DOPE (w/w). The circular dark areas correspond to the single defects. (B) The streptavidin molecules are trapped in the large defects of the annexin crystal and observed as bright spots. (C) Streptavidin molecules rapidly diffuse on the lipid bilayer without annexin and therefore they were observed as spike noises. For all images, the scan area is 200 nm × 200 nm and the buffer solution is 10mM HEPES-NaOH (pH 6.8), 20 mM NaCl, 150 mM KOAc, 2mM $MgCl_2$ and 2mM $CaCl_2$.

5. Protein 2D crystals as targets to study

5.1. Streptavidin 2D crystals

As mentioned in Section 3.2.3, the *C*222 and *P*2 crystals of streptavidin are not stable. Monovacancy defects are formed by increasing the tapping force exerted from an oscillating tip. The defects in the *C*222 crystal move in the plane, and this diffusion exhibits anisotropy correlated with the two crystallographic axes in the orthorhombic *C*222 crystal (Fig. 9A, B) (Yamamoto *et al*., 2008); one axis (a-axis) is comprised of contiguous biotin-bound subunit pairs whereas the other axis (b-axis) is comprised of contiguous biotin-unbound subunit pairs (Fig. 9C). The diffusivity along the b-axis is approximately 2.4 times larger than that along the a-axis. This anisotropy is ascribed to the difference in the free energy of association between the biotin bound and not biotin bound subunit-subunit interaction. A preferred intermolecular contact occurs between the not biotin bound subunits. The difference in the intermolecular binding free energy between the two types of subunit pairs is estimated from the ratio of diffusion constants to approximately 0.52 kcal/mole. Another dynamic behavior observed for point defects is the fusion of two point defects into a larger defect, which occurs much more frequently than the fission of a point defect into smaller defects (Fig. 9D). The diffusivity of point defects increases with increasing defect size. Fusion and higher diffusivity of larger defects are suggested to be involved in the mechanism of defect-free crystal formation.

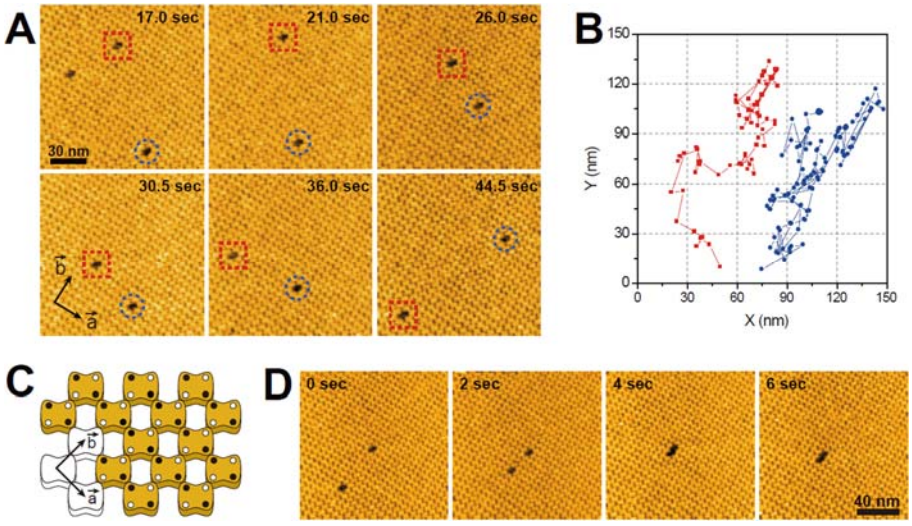

Figure 9. Diffusion of monovacancy defects in streptavidin *C*222 crystal observed by high-speed AFM (Yamamoto *et al*., 2008). (A) High-speed AFM images of the streptavidin 2D crystal and monovacancy defects migrating in the crystal. The monovacancy defects in the crystal are enclosed by the dashed squares (red) and circles (blue). The arrows indicate the direction of the lattice vectors of the crystal. Successive images were obtained at an imaging rate of 0.5 s/frame with 200 × 200 pixels. (B) Trajectories of the monovacancy defects obtained from the successive images (A). Closed squares (red) and circles (blue) correspond to defects enclosed by the open squares and circles in (A), respectively. (C) Schematic of streptavidin *C*222 crystal. The closed circles indicate biotin-bound subunits of streptavidin in the crystal, while the open circles correspond to biotin-unbound subunits. (D) Fusion of monovacancy defects in the *C*222 crystal. Two monovacancy defects migrate independently in the crystal at 0–2 sec, and then fused to form a divacancy defect at 4 sec. The resultant divacancy defect continued to migrate in the crystal (4–6 sec). The successive images were obtained at an imaging rate of 0.5 s/frame with 200 × 200 pixels.

5.2. p97 2D crystals

A multifunctional AAA ATPase, p97, is involved in cellular processes such as membrane fusion (Rabouille *et al*., 1998, Hetzer *et al*., 2001) and extraction of proteins from the endoplasmic reticulum for cytoplasmic degradation (Ye *et al*., 2001, Jarosch *et al*., 2002). Each subunit of the hexameric p97 contains two AAA domains (N-terminal D1 and C-terminal D2) and a flexible N-domain (Huyton *et al*., 2003). Its conformational changes during the ATPase cycle have been studied using cryo-EM and single-particle analysis in the presence of analogues of ATP hydrolysis products (Rouiller *et al*., 2002). It has been suggested that the relative positioning of the ring-shaped D1 and D2 domains changes and the N-domain moves in a direction perpendicular to the ring planes. We sought to prepare 2D crystals of p97 on Ni-NTA-containing lipid bilayers using a p97 with His-tag at the N-terminus of each subunit. It did not form crystals at neutral pH, but formed a crystal at acidic pH. Interestingly, p97 placed in an end-up orientation showed fluctuations in the height even in the absence of nucleotides (Fig. 10), suggesting that the N-domain assumes two conformations in equilibrium (unpublished). This conformational equilibrium probably shifts to one of the two states depending on the intermediate in the ATPase cycle, which is likely a process needed to extract proteins from the endoplasmic reticulum.

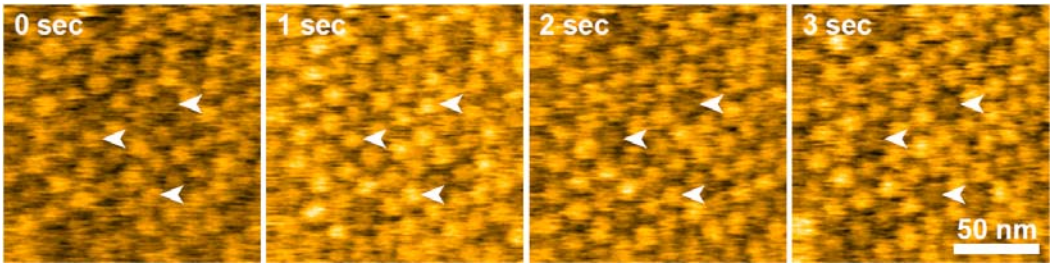

Figure 10. High speed AFM images of two-dimensional crystal of p97 having his-tag at the N-terminus, which was formed on Ni-NTA containing highly fluidic lipid bilayer. The crystal was formed under acidic pH (pH 5.6). The height of p97 fluctuates relative to other molecules in the crystal (arrowheads). Successive images were obtained at an imaging rate of 0.5 s/frame with 256×256 pixels.

5.3. Bacteriorhodopsin 2D crystals

In the purple membrane (PM) of *Halobacterium salinarum*, bacteriorhodopsin (bR) monomers associate to form a trimeric structure, and the trimers arrange in a hexagonal lattice (Henderson *et al*., 1990). The 2D crystals of bR and any crystals in general are in dynamic equilibrium with the constituents at the interface between crystal and liquid. High-speed AFM movies of the crystal edge of PM directly revealed this dynamic equilibrium (Fig. 11). Binding of trimeric bR predominates (82%), whereas binding of dimeric and monomeric bR is much less frequent, indicating that trimers are pre-formed in the non-crystalline region. The residence time of newly bound bR trimers at the crystal edge depends on the number of interaction sites. Within the two-dimensional bR crystal, a

trimer can interact with the surrounding trimers through six sites, whereas the number of interaction sites at the crystal edge is reduced to 1, 2, or 3, depending on the binding position of a newly bound trimer. From the ratio of the average residence times (0.19 s and 0.85 s) of two bound species containing two or three bonds, the elementary association energy is estimated to about –1.5 k_BT, which corresponds to –0.9 kcal/mol at 300 K (Yamashita *et al*., 2009).

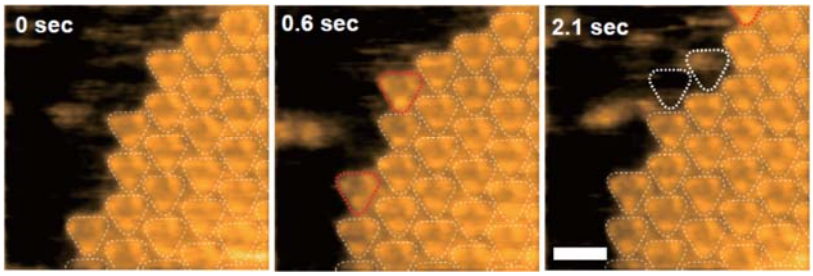

Figure 11. Dynamics at the crystal edge of bacteriorhodopsin in purple membrane (Yamashita *et al*., 2008). The AFM images were taken at 3.3 frames/s (scale bar, 10 nm). The bR molecules encircled by the red dotted lines indicate newly bound bR trimer. The white triangles (at 2.1 s) indicate the previously bound trimers.

6. Low-invasive imaging

In tapping mode high-speed AFM, the lateral force exerted from an oscillating cantilever tip to a sample is very small even when an image is taken within 30 ms (scan lines, ~100). High-speed AFM for biological samples requires small cantilevers with a high resonant frequency (~1 MHz) and a relatively small spring constant (0.1-0.2 N/m). With high frequency oscillations, the cantilever tip makes contact with a sample for only a very short time (~100 ns). During this virtually instantaneous contact, the sample stage is displaced only by < 0.2 nm as long as the scan range is < 300 nm, and hence, deformation of the sample in the lateral direction is negligible. On the other hand, the vertical force (tapping force) should be reduced by combining the various protocols and devices described in the following. This is mandatory for visualizing delicate biomolecular processes.

1. The free oscillation amplitude of a cantilever is optimized so that the tapping force is reduced and the feedback operation is not slowed down significantly. For very delicate samples, the amplitude has to be set at < 2 nm, sacrificing the feedback speed to some extent.
2. The amplitude set point should be set close to the free oscillation amplitude (> 90% of the free oscillation amplitude). Tip parachuting, which often occurs under this condition at the steep downhill regions of the sample, can be avoided using a dynamic proportional-integral-derivative (PID) controller (Kodera *et al*., 2006). In this controller, the gain parameters can be adjusted automatically and dynamically depending on the cantilever oscillation amplitude.
3. The free oscillation amplitude of a cantilever has to be maintained precisely constant. Otherwise, the tip-sample distance (hence, the tapping force) changes with time even when the cantilever

amplitude is maintained during imaging at the set point. Since the difference between the free oscillation amplitude and the set point is less than 0.2-0.3 nm under a very weak tapping force, even small drifts toward smaller free oscillation amplitude easily result in complete tip-sample detachment. This problem can be solved by a compensator for drift in the free oscillation amplitude (Kodera *et al.*, 2006). This compensator controls the AC voltage applied to a cantilever-excitation piezoactuator to maintain a constant second harmonic amplitude of the cantilever.

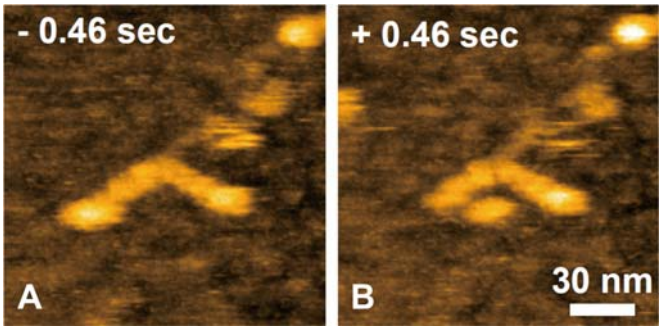

Figure 12. Structural change in myosin V upon uncaging calcium from caged-calcium. Calcium was released from caged-calcium at 0 sec. (A) Before UV illumination, (B) after UV illumination. The AFM images were taken at 464 ms/frame.

7. UV flash photolysis of caged compounds

UV flash photolysis of caged compounds is useful to detect minute structural changes of proteins induced by the interaction with chemicals such as ATP and calcium. Detected structural changes that are synchronized with the flash illumination can be concluded to be caused by the action of the uncaged chemical, facilitating distinction from Brownian motion. After irradiating a small area around the imaging area by a number of high-frequency UV flashes, the concentration of uncaged compound at the imaging area quickly decreases by rapid diffusion of the chemical. Therefore, repeated observation of structural changes is possible when they are reversible.

For a successful observation, the following precautions are required because UV illumination is prone to disturb the oscillation of a cantilever or to displace the sample stage by thermal expansion.

1. Use high-frequency weak UV pulses (~0.1 μJ/pulse) instead of a single shot of strong flash. A Nd:YVO4 355 nm laser with a repetition frequency > 50 kHz is commercially available.
2. Apply laser pulses while the y-scan is performed, near the starting point following acquisition of a frame.
3. Withdraw the sample stage from the cantilever tip during the y-scan.

Using a calcium-binding protein, CaM, attached to the neck region of MyoV, we here demonstrate high-speed AFM imaging combined with flash-photolysis of caged calcium. Each neck region of MyoV comprised of 6 IQ motifs to which six light chains (5 CaM and an essential light chain) are

attached. It is known that CaM attached to the second IQ dissociates in the presence of Ca^{2+} at micromolar concentrations (Koide et al., 2006). To facilitate the observation of structural changes induced in MyoV by CaM dissociation, MyoV was weakly attached to an aminosilane-coated mica surface on which the neck regions can extend (Fig. 12A). On each neck region, three small globes corresponding to three light chains are visible, but the other three light chains face the mica surface. Just after the illumination by ~100 UV pulses of 100 kH frequency, one of the motor domains (a large globe) located at the distal end of the head partially dissociates from the adjacent neck region (Fig. 12B), but the three globes on the neck remain visible. Probably one of the three light chains facing the mica surface dissociated from the neck. The partially dissociated motor domain was observed to be linked to the neck region through a thin structure. This behavior was rather rare among many observations. The observations mostly showed shrinkage of the neck region after UV illumination, suggesting folding of an exposed IQ motif after dissociation of CaM.

8. Cantilever tip

Finally, high spatial resolution is also important in high-speed AFM. The resolution is mainly determined by the apex radius and the aspect ratio of a cantilever tip, in addition to the performance of the instrument. Thus far, small cantilevers with a sharp tip are not commercially available. Piece-by-piece attachment of a carbon nanotube to a cantilever tip is possible (Dai, 1996). However, this laborious attachment cannot be routinely performed. Instead, we have employed electron beam deposition (EBD) to grow a carbon tip on the original tip (Wendel, 1995). A piece of phenol crystal (sublimate) is placed in a small container with small holes (~0.1 mm diameter) in the lid. The container is placed in a scanning electron microscope chamber and small cantilevers are placed above the holes. A spot-mode electron beam is focused onto each original tip, which produces a needle on the original tip at a growth rate of ~17 nm/s. The newly formed carbon tip has an apex radius of 15–25 nm (Fig. 13A, B) and is sharpened by plasma etching in argon or oxygen gas, which decreases the apex radius to 4-5 nm (Fig. 13C).

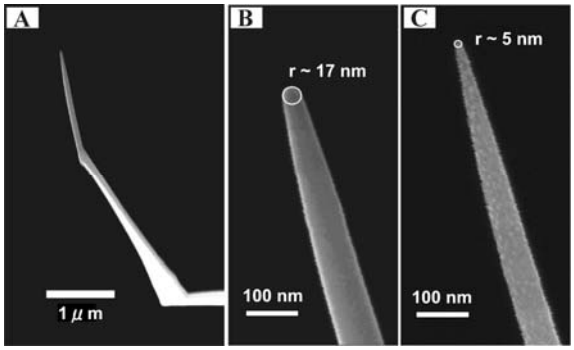

Figure 13. (A) A SEM image of an EBD tip grown from phenol as a vapor source. The deposition time was 90 s. The electron energy, working distance and aperture size of the FE-SEM during the deposition were 20 kV, 4mm and 30 μm, respectively. (B) The apex radius of the grown tip is about 17 nm. (C) After etching in Ar gas for 8 min using a plasma etcher with the power of 16 W, the apex radius is reduced to about 5 nm.

References

Ando, T., Kodera, N., Takai, E., Maruyama, D., Saito, K., and Toda, A. (2001). A high-speed atomic force microscope for studying biological macromolecules. *Proc. Natl. Acad. Sci. U.S.A.* **98**, 12468–12472.

Ando, T., Kodera, N., Maruyama, D., Takai, E., Saito, K., and Toda, A. (2002). A High-speed atomic force microscope for studying biological macromolecules in action. *Jpn. J. Appl. Phys.* **41**, 4851–4856.

Ando, T., Uchihashi, T., Kodera, N., Miyagi, A., Nakakita, R., Yamashita, H., and Sakashita, M. (2006). High-speed atomic force microscopy for studying the dynamic behavior of protein molecules at work. *Jpn. J. Appl. Phys*. **45**, 1897–1903.

Ando, T., Uchihashi, T., and Fukuma, T. (2008). High-speed atomic force microscopy for nano-visualization of dynamic biomolecular processes. *Prog. Surf. Sci.* **83.** 337–437.

Dai, H., Hafner, J. H., Rinzler, A. G., Colbert, D. T. R., and Smalley, E. (1996). Nanotubes as nanoprobes in scanning probe microscopy. *Nature* **384**, 147–150.

Darst, S. A. , Ahlers, M., Meller, P. H., Kubalek, E. W., Blankenburg, R., Ribi, H. O., Ringsdorf, H., and Kornberg, R. D. (1991). Two-dimensional crystals of streptavidin on biotinylated lipid layers and their interactions with biotinylated macromolecules. *Biophys. J.* **59**, 387–396.

Fantner, G. E., Schitter, G., Kindt, J. H., Ivanov, T., Ivanova, K., Patel, R., Holten-Andersen, N., Adams, J., Thurner, P. J., Rangelow, I. W., and Hansma, P. K. (2006). Components for high speed atomic force microscopy. *Ultramicroscopy* **106**, 881–887.

Goldman, Y. E. (2009). Imaging and molecular motors. *In* "Single molecule dynamics in life science" (T. Yanagida and Y. Ishii, eds.), Wiley-VCH, Weinheim, 2009, pp. 41-85.

Green, N. M. (1990). Avidin and streptavidin. *Methods Enzymol.* **184**, 51–67.

Henderson, R., Baldwin, J. M., Ceska, T. A., Zemlin, F., Beckmann, E., Downing, K. H. (1990). Model for the structure of bacteriorhodopsin based on high-resolution electron cryo-microscopy. *J. Mol. Biol.* **213**, 899–929.

Hetzer, M., Meyer, H. H., Walther, T. C., Bilbao-Cortes, D., Warren, G., and Mattaj, I. W. (2001). Distinct AAA-ATPase p97 complexes function in discrete steps of nuclear assembly. *Nat. Cell Biol.* **3**, 1086–1091.

Heyes, C. D., Kobitski, A. Y., Amirgoulova, E. V., and Nienhaus, G. U. (2004). Biocompatible surfaces for specific tethering of individual protein molecules. *J. Phys. Chem. B* **108**, 13387–13394.

Hinterdorfer, P., and Dufrêne, Y. F. (2006). Detection and localization of single molecular recognition events using atomic force microscopy. *Nature Methods* **3**, 347–355.

Huang, B., Bates, M., and Zhuang, X. (2009). Super-resolution fluorescence microscopy. *Annu. Rev. Biochem*. **78**, 993-1016.

Huyton, T., Pye, V. E., Briggs, L. C., Flynn, T. C., Beuron, F., Kondo, H., Ma, J., Zhang, X., and

Freemont, P. S. (2003). The crystal structure of murine p97/VCP at 3.6Å. *J. Struct. Biol.* **144**, 337–348.

Ichikawa, T., Aoki, T., Takeuchi, Y., Yanagida, T., and Ide,T. (2006). Immobilizing single lipid and channel molecules in artificial lipid bilayers with annexin A5. *Langmuir* **22**, 6302–6307.

Jarosch, E., Taxis, C., Volkwein, C., Bordallo, J., Finley, D., Wolf, D. H., and Sommer, T. (2002). Protein dislocation from the ER requires polyubiquitination and the AAA-ATPase Cdc48. *Nat. Cell Biol.* **4**, 134–139.

Joo, C., Balci, H., Ishitsuka, Y., Buranachai, C., and Ha, T. (2008). Advances in Single-Molecule Fluorescence Methods for Molecular Biology. *Annu. Rev. Biochem*. **77**, 51-76.

Kodera, N., Yamashita, H., and Ando, T. (2005). Active damping of the scanner for high-speed atomic force microscopy. *Rev. Sci. Instrum.* **76,** 053708.

Kodera, N., Sakashita, M., and Ando, T. (2006). Dynamic proportional-integral-differential controller for high-speed atomic force microscopy. *Rev. Sci. Instrum*. **77**, 083704.

Koide H., Kinoshita, T., Tanaka, Y., Tanaka, S., Nagura, N., zu Hörste, G. M., Miyagi, A., and Ando, T. (2006). Identification of the specific IQ motif of myosin V from which calmodulin dissociates in the presence of Ca^{2+}. *Biochemistry* **45,** 11598-11604.

Liu, M., Amro, N. A., and Liu, G.-Y. (2008). Nanografting for Surface: Physical Chemistry. *Annu. Rev. Phys. Chem*. **59**, 367–386.

Miyagi, A., Tsunaka, Y., Uchihashi, T., Mayanagi, K., Hirose, S., Morikawa, K., and Ando, T. (2008). Visualization of intrinsically disordered regions of proteins by high-speed atomic force microscopy. *Chem. Phys. Chem*. **9**, 1859–1866.

Park, H., Toprak, E., and Selvin, P. R. (2007). Single-molecule fluorescence to study molecular motors. *Quat. Rev. Biophys*. **40**, 87-111.

Rabouille, C., Kondo, H., Newman, R., Hui, N., Freemont, P., and Warren, G. (1998). Syntaxin 5 is a common component of the NSF- and p97-mediated reassembly pathways of Golgi cisternae from mitotic Golgi fragments in vitro. *Cell* **92**, 603–610.

Ratanabanangkoon, P., and Gast, A. P. (2003). Effect of ionic strength on two-dimensional streptavidin crystallization. *Langmuir* **19**, 1794–1801.

Reviakine, I., and Brisson, A. (2001). Streptavidin 2D crystals on supported phospholipid bilayers: toward constructing anchored phospholipid bilayers. *Langmuir* **17**, 8293-–299.

Richter, R. P., Him, J. L. K., Tessier, B., Tessier, C., and Brisson, A. R. (2005). On the Kinetics of Adsorption and Two-Dimensional Self-Assembly of Annexin A5 on Supported Lipid Bilayers. *Biophys. J*. **89**, 3372–3385.

Rouiller, I., DeLaBarre, B., May, A. P., Weis, W. I., Brunger, A. T., Milligan, R. A., and Wilson-Kubalek, E. M. (2002). Conformational changes of the multifunction p97 AAA ATPase during

its ATPase cycle. *Nat. Struct. Biol.* **9**, 950–957.

Scheuring, S., Müller, D. J., Ringler, P., Heymann, J. B., and Engel, A. (1999). Imaging streptavidin 2D crystals on biotinylated lipid monolayers at high resolution with the atomic force microscope. *J. Microscopy* **193**, 28–35.

Shibata, M., Yamashita, H., Uchihashi, T., Kandori H., and Ando, T. High-speed atomic force microscopy visualization reveals dynamic molecular processes in photo-activated bacteriorhodopsin. *Nature Nanotech*. (submitted).

Vadgama, P. (2005). Surface biocompatibility. *Annu. Rep. Prog. Chem., Sect. C: Phys. Chem*. **101**, 14–52.

Viani, M.B., Schäffer, T. E., Paloczi, G. T., Pietrasanta, L. I., Smith, B. L., Thompson, J. B., Richter, M., Rief, M., Gaub, H. E., Plaxco, K. W., Cleland, A. N., Hansma, H. G., and Hansma, P. K. (1999). Fast imaging and fast force spectroscopy of single biopolymers with a new atomic force microscope designed for small cantilevers. *Rev. Sci. Instrum*. **70**, 4300–4303.

Wang, S.-W., Robertson, C. R., and Gast, A. P. (1999). Molecular arrangement in two-dimensional streptavidin crystals. *Langmuir* **15**, 1541–1548.

Wendel, M., Lorenz, H., and Kotthaus, J. P. (1995). Sharpened electron beam deposited tips for high resolution atomic force microscope lithography and imaging. *Appl. Phys. Lett.* **67**, 3732.

Yamamoto, D., Uchihashi, T., Kodera, N., and Ando, T. (2008). Anisotropic diffusion of point defects in two-dimensional crystal of streptavidin observed by high-speed atomic force microscopy. *Nanotechnol*. **19**, 384009.

Yamamoto, D., Nagura, N., Omote, S., Taniguchi, M., and Ando, T. (2009). Streptavidin 2D crystal substrates for visualizing biomolecular processes by atomic force microscopy. *Biophys. J*. (in press).

Yamashita, H., Uchihashi, T., Kodera, N., Miyagi, A., Yamamoto, D., and Ando, T. (2007). Tip-sample distance control using photo-thermal actuation of a small cantilever for high-speed atomic force microscopy. *Rev. Sci. Instrum.* **78**, 083702.

Yamashita, H., Voïtchovsky, K., Uchihashi, T., Antoranz Contera, S., Ryan, J. F., and Ando, T. (2009). Dynamics of bacteriorhodopsin 2D crystal observed by high-speed atomic force microscopy. *J. Struct. Biol*. **167,** 153-158.

Ye, Y., Meyer, H. H., and Rapoport, T. A. (2001). The AAA ATPase Cdc48/p97 and its partners transport proteins from the ER into the cytosol. *Nature* **414**, 652–656.

Zhang, S. F., Rolfe, P., Wright, G., Lian, W., Milling, A. J., Tanaka, S., and Ishihara, K. (1998). Physical and biological properties of compound membranes incorporating a copolymer with a phosphorylcholine head group. *Biomater*. **19**, 691–700.